

Ultradense dark matter haloes accompanying primordial black holes

M. Sten Delos,^{1*} Joseph Silk²

¹ *Max Planck Institute for Astrophysics, Karl-Schwarzschild-Str. 1, 85748 Garching, Germany*

² *Institut d'Astrophysique de Paris, UMR7095:CNRS UPMC-Sorbonne University, F-75014, Paris, France*

Accepted XXX. Received YYY; in original form ZZZ

ABSTRACT

Primordial black holes (PBHs) form from large-amplitude initial density fluctuations and may comprise some or all of the dark matter. If PBHs have an extended mass spectrum, or in mixed PBH-particle dark matter scenarios, the extreme density fluctuations necessary to produce PBHs also lead to the formation of a much greater abundance of dark matter minihaloes with internal densities potentially of order $10^{12} \text{ M}_{\odot} \text{ pc}^{-3}$. We develop an analytic description of the formation of these ultradense haloes and use it to quantitatively compare PBH and halo distributions. PBHs that contribute only a per cent level fraction of the dark matter are accompanied by ultradense haloes that nevertheless comprise an order-unity fraction. This finding significantly alters the predictions of many PBH scenarios, enabling a variety of new observational tests.

Key words: cosmology: theory – dark matter – early Universe – methods: analytical

1 INTRODUCTION

Primordial black holes (PBHs) are an attractive dark matter candidate (Carr & Kühnel 2020; Green & Kavanagh 2021). They form deep in the radiation-dominated epoch from large-amplitude initial density fluctuations, which occur on scales too small to influence precision cosmological observables like the large-scale galaxy distribution and temperature variations in the cosmic microwave background. In addition to the possibility that they comprise some or all of the dark matter, PBHs have been proposed to explain binary black hole coalescence detections by the LIGO/Virgo/KAGRA (LVK) collaboration (e.g. Bird et al. 2016; Sasaki et al. 2016) and to act as seeds for the supermassive black holes found at the centres of galaxies (e.g. Carr & Silk 2018).

An array of observational constraints significantly limit the possibility that PBHs in a narrow mass range comprise most of the dark matter (Carr et al. 2021b). However, extended PBH mass spectra remain viable, as do mixed scenarios with PBHs and particle dark matter. For example, while some properties of black hole systems seen in LVK observations (e.g. Abbott et al. 2020) are difficult to realize with stellar black holes, they can be explained if PBHs around 10 to 100 M_{\odot} contribute to the dark matter at the sub-per cent level (Franciolini et al. 2022). Similar PBH mass fractions can seed supermassive black holes (Carr & Silk 2018), which are also challenging to explain through astrophysical formation channels (Volonteri et al. 2021). Extended PBH mass spectra that explain either or both phenomena can arise naturally from the timing of phase transitions in the early universe (Byrnes et al. 2018; Carr et al. 2021a; Escrivà et al. 2022).

In mixed scenarios with PBHs and particle dark matter, and in PBH scenarios with broadly extended mass functions, dark matter is present when PBHs are forming. Whereas PBHs form from extreme $O(1)$ variations in the primordial density, weaker fluctuations that

fail to form PBHs are far more common. These fluctuations are still sufficient to induce the formation of dark matter haloes long before they would be otherwise expected to form. Due to their early formation, these haloes would have extraordinarily high internal density. In particular, ultradense haloes can arise via the collapse of overdense regions deep in the radiation epoch.

This brief note develops an analytic description of ultradense halo formation and presents quantitative comparisons of PBH and ultradense halo populations. The idea that such haloes should vastly outnumber PBHs was considered previously by Ricotti & Gould (2009) and Kohri et al. (2014), but the model of halo formation and structure employed therein disagrees with later numerical simulation results (Gosenca et al. 2017; Delos et al. 2018a,b). These works also restricted their consideration to haloes forming during the last matter-dominated epoch. In contrast, Kolb & Tkachev (1994), Dokuchaev & Eroshenko (2002), and Berezhinsky et al. (2010, 2013) studied halo formation during the radiation epoch using models of spherical and ellipsoidal collapse. Motivated by a recent simulation result (Blanco et al. 2019), we employ a related approach based on ellipsoidal collapse and the notion that halo formation proceeds once a collapsed region becomes locally matter dominated.

We show that haloes forming by a redshift of around 10^5 can comprise an $O(1)$ fraction of the dark matter even when PBHs arising from fluctuations at the same scale contribute only at the per cent level. Such early formation yields internal halo densities of order $10^{12} \text{ M}_{\odot} \text{ pc}^{-3}$. The abundance of these ultradense haloes substantially alters the predictions of many PBH scenarios and enables a new range of observational tests.

2 FORMATION OF ULTRADENSE HALOES

During the radiation-dominated epoch, primordial curvature perturbations ζ at the scale wavenumber k cause linear-order dark matter

* E-mail: sten@mpa-garching.mpg.de

density perturbations δ to grow as

$$\delta(k, a) = I_1 \zeta(k) \log(I_2 a/a_H) = I_1 \zeta(k) \log\left(\sqrt{2} I_2 \frac{k}{k_{\text{eq}}} \frac{a}{a_{\text{eq}}}\right) \quad (1)$$

when $a \gg a_H$, where $a_H = 2^{-1/2}(k_{\text{eq}}/k)a_{\text{eq}}$ is the expansion factor at horizon entry, $I_1 \approx 6.4$, and $I_2 \approx 0.47$ (Hu & Sugiyama 1996). Here $a_{\text{eq}} \approx 3 \times 10^{-4}$ and $k_{\text{eq}} \approx 0.01 \text{ Mpc}^{-1}$ are the expansion factor and horizon scale at matter-radiation equality. The growth described by Eq. (1) arises solely due to drifting particles, which cover comoving distances logarithmic in a . The only gravitational kick arises from the transient peculiar potential at horizon entry, before the radiation pressure homogenizes it.

Since peculiar gravitational forces are negligible, an ellipsoidal collapse treatment is trivial because we can simply allow each axis to drift independently. In particular, if a region of scale k^{-1} has an initial (transient) tidal field with ellipticity e and prolateness p , then its density evolves as

$$\frac{\rho}{\rho_m} = \frac{1}{\prod_{i=1}^3 |1 - \lambda_i \delta(k, a)|}, \quad (2)$$

where ρ_m is the average dark matter density and $\lambda_1 = (1 + 3e + p)/3$, $\lambda_2 = (1 - 2p)/3$, and $\lambda_3 = (1 - 3e + p)/3$. The last axis collapses at the scale factor a_c when $\lambda_3 \delta(k, a_c) = 1$, i.e. at the critical linear density contrast

$$\delta_c = \frac{3}{1 - 3e + p}. \quad (3)$$

For a density contrast δ in a Gaussian random density field with rms contrast σ , the most probable values of e and p are $e = (\sqrt{5}\delta/\sigma)^{-1}$ and $p = 0$, respectively (Sheth et al. 2001). For example, a typical 3σ density peak has a collapse threshold of about $\delta_c \approx 5$. For such a peak to collapse by $a \approx 10a_H$ requires $\zeta \gtrsim 0.5$. However, only $\zeta \gtrsim 0.15$ is required to induce collapse of such a peak by $a \approx 300a_H$. In contrast, $\zeta \sim 1$ is required to form a primordial black hole (Green et al. 2004). Thus, it is already clear that minihaloes can potentially far outnumber primordial black holes.

However, the formation of haloes from collapsed structures cannot be taken for granted during the radiation epoch. Blanco et al. (2019) demonstrated in a numerical simulation that the collapse of a peak yields a virialized halo only when the collapsed region becomes locally matter dominated. Consequently, it is not guaranteed that a halo will form at the moment of collapse. On the other hand, Blanco et al. (2019) also noted that collapsed regions can be orders of magnitude denser than the dark matter average. In particular, we estimate in Appendix A that the density of a collapsed region is of order $\rho/\rho_m \sim e^{-2}$ times the mean matter density, where e is the ellipticity of the initial tidal field again. For the typical ellipticity $e \approx 0.15$ of the tidal field at a 3σ peak, local matter domination thus occurs at $a \sim e^2 a_{\text{eq}} \approx 0.02 a_{\text{eq}}$, leading to halo formation long before the matter-dominated epoch begins. Being proportional to the mean cosmic density at their formation time, the density inside these haloes would be extraordinarily high.

If we replace e and p in Eq. (3) by their most probable values, $e = (\sqrt{5}\delta_c/\sigma)^{-1}$ and $p = 0$, then we obtain the collapse threshold

$$\delta_c = 3 \left(1 + \sigma/\sqrt{5}\right) \quad (4)$$

as a function of σ . In the excursion set formalism (Bond et al. 1991), this threshold corresponds to the moving barrier

$$B(S) \equiv 3(1 + \sqrt{S/5}), \quad (5)$$

where $S \equiv \sigma^2$. For a Gaussian random walk, the distribution of first

barrier crossings in this scenario is well approximated by

$$F(S) = \frac{3 + 0.556\sqrt{S}}{\sqrt{2\pi}S^{3/2}} \exp\left[-\frac{B(S)^2}{2S}\right] \left(1 + \frac{S}{400}\right)^{-0.15}, \quad (6)$$

which we verified by Monte Carlo simulation. This distribution leads to the Press-Schechter halo mass function

$$\frac{dn}{d \log M} = \sqrt{\frac{2}{\pi}} \frac{(\nu + 0.556)e^{-\frac{1}{2}(\nu+1.34)^2}}{(1 + 0.0225\nu^{-2})^{0.15}} \frac{d \log \nu}{d \log M} \frac{\rho_{m,0}}{M}, \quad (7)$$

where $\rho_{m,0} \approx 33 \text{ M}_\odot \text{ kpc}^{-3}$ is the comoving dark matter density and $\nu \equiv 3/\sigma_M$. Here, σ_M is the rms density contrast smoothed on the mass scale M , which we evaluate using a sharp- k filter in order to accommodate power spectra that deviate significantly from scale invariance (Benson et al. 2013). That is,

$$\sigma_M^2 = \int_0^{k_M} \frac{dk}{k} \mathcal{P}(k, a) \quad (8)$$

with $M \equiv 6\pi^2 \rho_{m,0} k_M^{-3}$ (Lacey & Cole 1993), which implies also

$$\frac{d \log \nu}{d \log M} = \frac{\mathcal{P}(k_M, a)}{6\sigma_M^2}. \quad (9)$$

Here, $\mathcal{P}(k, a) \equiv [k^3/(2\pi^2)]P(k, a)$ is the dimensionless matter power spectrum, which is a function of time. In particular, Eq. (1) implies that

$$\mathcal{P}(k, a) = I_1^2 \left[\log\left(\sqrt{2} I_2 \frac{k}{k_{\text{eq}}} \frac{a}{a_{\text{eq}}}\right) \right]^2 \mathcal{P}_\zeta(k), \quad (10)$$

where $\mathcal{P}_\zeta(k)$ is the dimensionless power spectrum of primordial curvature perturbations.

Note that while we focused here on structure arising from curvature perturbations, halo formation from isocurvature perturbations during the radiation epoch (e.g. Kolb & Tkachev 1994) is even more favourable in comparison to PBH formation. For adiabatic curvature perturbations, haloes are disadvantaged in relation to PBHs by the requirement that local matter domination be achieved before peculiar gravitational forces become significant. PBHs, in contrast, can form from radiation perturbations alone. But in the case of structure arising from isocurvature perturbations, both the PBHs and the haloes form essentially out of matter, so the haloes are no longer so disadvantaged. Similar considerations apply to PBHs that form during an early matter-dominated phase (Belotsky et al. 2019).

3 ULTRADENSE HALOES AND PBHS

Due to the arguments above, ultradense minihaloes are generally expected to vastly outnumber PBHs in scenarios where there is dark matter present at the time that the PBHs form. This means that either

- (i) PBHs are only a fraction of the dark matter, or
- (ii) PBHs are all of the dark matter but have a broadly extended mass function.

In case (i), the haloes form out of particle dark matter, which we also require to have kinetically decoupled by the time PBHs are forming, so that the radiation pressure does not suppress clustering. In case (ii), the haloes form out of much smaller PBHs. Note that the PBH mass spectrum must then be weighted towards low masses, but such weighting is naturally expected to arise for broad primordial power spectra (De Luca et al. 2020a). We now discuss a couple of examples of the latter case.

As our first example, let us consider the scenario presented by

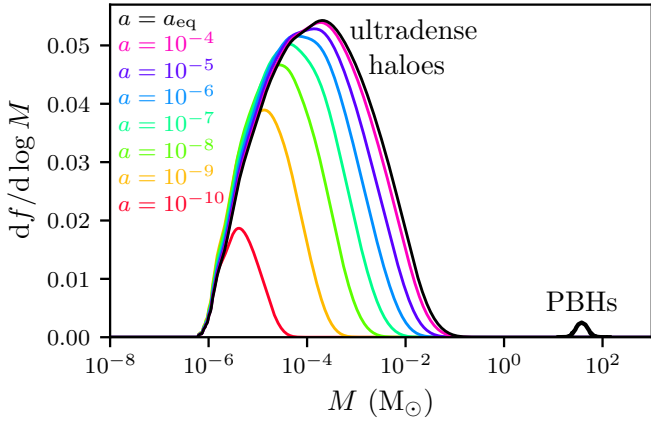


Figure 1. Differential dark matter mass fraction in ultradense haloes (left) and PBHs (right) in the double inflation scenario of Inomata et al. (2018). We consider haloes that form by matter-radiation equality (black) as well as regions that collapse by earlier times (colours); note that collapse precedes halo formation but does not necessarily induce it immediately. In total, these ultradense haloes in the range 10^{-6} to 10^{-1} M_{\odot} comprise roughly 40 per cent of the dark matter. In contrast, 10 to 100 M_{\odot} PBHs, which form from fluctuations at the same scale, comprise only about 0.2 per cent of the dark matter.

Inomata et al. (2018). Here, a double inflation model yields a complicated primordial power spectrum that produces asteroid-mass PBHs that comprise almost all of the dark matter while also producing a small abundance of 10 to 100 M_{\odot} PBHs to explain LVK binary coalescence detections (e.g. Abbott et al. 2016). We then expect that the density variations that produce the 10 to 100 M_{\odot} PBHs also create ultradense minihaloes consisting of asteroid-mass PBHs. In particular, Fig. 1 shows the differential mass fraction $df/d \log M = (M/\rho_{m,0})dn/d \log M$ in ultradense haloes that form during the radiation epoch; note that we include only haloes that form from the largest-scale spike in the primordial power spectrum (which is the same for both models presented in Inomata et al. 2018). In total, 10 to 100 M_{\odot} PBHs comprise only about 0.2 per cent of the dark matter, but the boosted density variations necessary to produce them cause about 40 per cent of the dark matter mass to reside in ultradense haloes between earth mass and solar mass. Note that for adiabatic initial fluctuations, individual ultradense haloes are generically expected to be somewhat less massive than PBHs arising at the same length scale because haloes form from matter, which is a/a_{eq} times as abundant as the radiation that produces PBHs.

We next consider the scenario of Carr et al. (2021a). Here, the primordial power spectrum is

$$\mathcal{P}_{\zeta}(k) = \begin{cases} A_s [k/(0.05 \text{ Mpc}^{-1})]^{n_s-1} & \text{if } k < k_1 \\ A_1 [k/(10^6 \text{ Mpc}^{-1})]^{n_s-1} & \text{if } k > k_1, \end{cases} \quad (11)$$

where $A_s = 2.1 \times 10^{-9}$ and $n_s = 0.96$ to match data from the cosmic microwave background (Planck Collaboration et al. 2020), but the power is boosted to $A_1 \approx 0.022$ at small scales $k > k_1 \approx 90 \text{ Mpc}^{-1}$ in order to produce PBHs in the right abundance to comprise all of the dark matter. This spectrum is featureless and scale invariant for $k > k_1$, but it yields the nontrivial PBH mass function shown in Fig. 2 due to the nontrivial thermal history of the early universe. In this scenario, the bulk of the dark matter consists of $O(1) M_{\odot}$ PBHs, but a tail of much larger PBHs act as seeds for the supermassive black holes found at the centres of galaxies. However, density variations on scales large enough to produce such PBHs also cause the solar mass

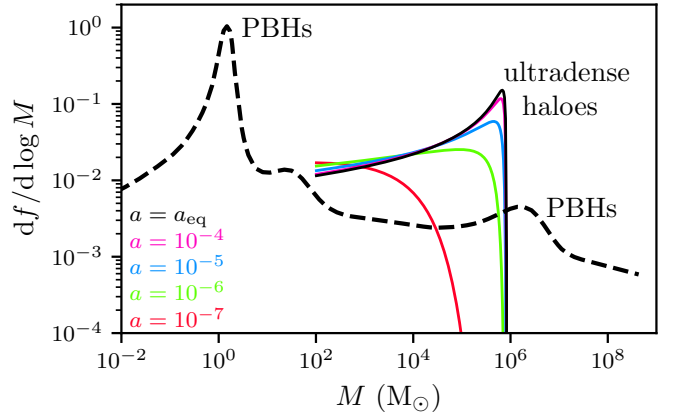


Figure 2. Differential dark matter mass fraction in ultradense haloes (solid curves) and PBHs (dashed curve) in the PBH scenario of Carr et al. (2021a). We consider haloes that form by matter-radiation equality (black) as well as regions that collapse by earlier times (colours). The tail of PBHs larger than $10^3 M_{\odot}$ act as supermassive black hole seeds, but this tail is accompanied by an abundance of ultradense haloes that form out of much smaller $O(1) M_{\odot}$ PBHs. About 30 per cent of the dark matter resides in ultradense haloes larger than $10^3 M_{\odot}$.

PBHs to cluster into ultradense haloes up to $O(10^6) M_{\odot}$. Whereas PBHs larger than $10^3 M_{\odot}$ comprise only 3 per cent of the dark matter, 30 per cent of the dark matter resides in ultradense haloes above this mass scale.

In Figs. 1 and 2, we show not only the halo distribution at matter-radiation equality (in black) but also the distribution of collapsed regions at earlier times (colours). A halo’s internal density is of order 10^3 times the density of the universe at its formation time a_f (Delos & White 2022a), i.e.

$$\rho_{\text{halo}} \sim 10^3 (1 + a_{eq}/a_f) a_f^{-3} \rho_{m,0}, \quad (12)$$

where $\rho_{m,0} \approx 33 M_{\odot} \text{ kpc}^{-3}$ is again the comoving dark matter density. As we discussed in Section 2, a halo’s formation time a_f is not necessarily the time a_c at which its precursor mass distribution collapsed, but halo formation can in general occur orders of magnitude earlier than matter-radiation equality. Since the coloured curves in Figs. 1 and 2 are selected by a_c and not a_f , they do not directly inform us of the density of the resulting haloes, but we may note that in both scenarios the distribution of collapsed regions at $a = 10^{-5}$ is comparable to that at $a = a_{eq}$. Since collapsed regions can typically form haloes by $a = 10^{-5} \approx a_{eq}/30$ (see Section 2), most of the ultradense haloes are expected to have formation times $a_f < 10^{-5}$, implying internal densities $\rho_{\text{halo}} \gtrsim 10^{12} M_{\odot} \text{ pc}^{-3}$. These ultradense haloes are about 10^{12} times denser than the first haloes that would form around redshift 30 in a standard cold dark matter cosmology (e.g. Delos & White 2022b) and of order 10^{19} times denser than the cosmological mean today.

4 CONCLUSION

If PBHs have a broad mass function, or if they comprise only a fraction of the dark matter, then they are expected to be accompanied by ultradense minihaloes with internal densities of order 10^{12} times that of standard cold dark matter haloes. These ultradense haloes form during the radiation-dominated epoch from large-amplitude initial density variations similar to those that are necessary to produce

PBHs. However, the haloes comprise an $O(1)$ fraction of the dark matter even when PBHs arising at the same length scales contribute only at the per cent level.

For PBHs in the 10 to 100 M_{\odot} mass range, which have been suggested to explain LVK observations, ultradense haloes are produced in the earth-mass to solar-mass range. Such minihaloes can be detected by pulsar timing distortions (Dror et al. 2019) or gravitational lensing (Erickcek & Law 2011; Croon et al. 2020; Dai & Miralda-Escudé 2020). Much larger PBHs, which could act as seeds for supermassive black holes, are accompanied by ultradense haloes potentially up to 10^3 to $10^6 M_{\odot}$. These haloes are sufficiently massive that they could produce dynamical signatures within galaxies (Delos & Schmidt 2022) and even affect early galaxy formation (Inman & Kohri 2022). In mixed dark matter scenarios with PBHs and thermal relics, ultradense haloes would also enormously boost the dark matter annihilation rate, potentially leading to detectable gamma rays (Bringmann et al. 2012) or other signatures (e.g. Clark et al. 2017; Silk 2018), although these mixed scenarios are already tightly constrained (Adamek et al. 2019). For broad PBH mass spectra, the presence of ultradense haloes implies that PBHs quickly become highly clustered, even if they are not clustered at formation (Moradinezhad Dizgah et al. 2019). Such clustering can significantly impact the binary coalescence rate (Bringmann et al. 2019; Raidal et al. 2019; De Luca et al. 2020b). Thus, the ultradense haloes that accompany PBH formation enable an array of new tests of PBH scenarios.

ACKNOWLEDGEMENTS

We thank Fabian Schmidt and Eiichiro Komatsu for helpful comments on the manuscript.

DATA AVAILABILITY

No datasets were created or analysed during this study.

REFERENCES

- Abbott B. P., et al., 2016, *Physical Review X*, 6, 041015
 Abbott R., et al., 2020, *Phys. Rev. Lett.*, 125, 101102
 Adamek J., Byrnes C. T., Gosenca M., Hotchkiss S., 2019, *Phys. Rev. D*, 100, 023506
 Belotsky K. M., et al., 2019, *European Physical Journal C*, 79, 246
 Benson A. J., et al., 2013, *MNRAS*, 428, 1774
 Berezhinsky V., Dokuchaev V., Eroshenko Y., Kachelrieß M., Solberg M. A., 2010, *Phys. Rev. D*, 81, 103529
 Berezhinsky V. S., Dokuchaev V. I., Eroshenko Y. N., 2013, *J. Cosmology Astropart. Phys.*, 2013, 059
 Bird S., Cholis I., Muñoz J. B., Ali-Haïmoud Y., Kamionkowski M., Kovetz E. D., Raccanelli A., Riess A. G., 2016, *Phys. Rev. Lett.*, 116, 201301
 Blanco C., Delos M. S., Erickcek A. L., Hooper D., 2019, *Phys. Rev. D*, 100, 103010
 Bond J. R., Cole S., Efstathiou G., Kaiser N., 1991, *ApJ*, 379, 440
 Bringmann T., Scott P., Akrami Y., 2012, *Phys. Rev. D*, 85, 125027
 Bringmann T., Depta P. F., Domcke V., Schmidt-Hoberg K., 2019, *Phys. Rev. D*, 99, 063532
 Byrnes C. T., Hindmarsh M., Young S., Hawkins M. R. S., 2018, *J. Cosmology Astropart. Phys.*, 2018, 041
 Carr B., Kühnel F., 2020, *Annual Review of Nuclear and Particle Science*, 70, 355
 Carr B., Silk J., 2018, *MNRAS*, 478, 3756

- Carr B., Clesse S., García-Bellido J., Kühnel F., 2021a, *Physics of the Dark Universe*, 31, 100755
 Carr B., Kohri K., Sendouda Y., Yokoyama J., 2021b, *Reports on Progress in Physics*, 84, 116902
 Clark H. A., Iwanus N., Elahi P. J., Lewis G. F., Scott P., 2017, *J. Cosmology Astropart. Phys.*, 2017, 048
 Croon D., McKeen D., Raj N., 2020, *Phys. Rev. D*, 101, 083013
 Dai L., Miralda-Escudé J., 2020, *AJ*, 159, 49
 De Luca V., Franciolini G., Riotto A., 2020a, *Physics Letters B*, 807, 135550
 De Luca V., Desjacques V., Franciolini G., Riotto A., 2020b, *J. Cosmology Astropart. Phys.*, 2020, 028
 Delos M. S., Schmidt F., 2022, *MNRAS*, 513, 3682
 Delos M. S., White S. D. M., 2022a, arXiv e-prints, p. arXiv:2207.05082
 Delos M. S., White S. D. M., 2022b, arXiv e-prints, p. arXiv:2209.11237
 Delos M. S., Erickcek A. L., Bailey A. P., Alvarez M. A., 2018a, *Phys. Rev. D*, 97, 041303
 Delos M. S., Erickcek A. L., Bailey A. P., Alvarez M. A., 2018b, *Phys. Rev. D*, 98, 063527
 Dokuchaev V. I., Eroshenko Y. N., 2002, *Soviet Journal of Experimental and Theoretical Physics*, 94, 1
 Dror J. A., Ramani H., Trickle T., Zurek K. M., 2019, *Phys. Rev. D*, 100, 023003
 Erickcek A. L., Law N. M., 2011, *ApJ*, 729, 49
 Escrivà A., Bagui E., Clesse S., 2022, arXiv e-prints, p. arXiv:2209.06196
 Franciolini G., et al., 2022, *Phys. Rev. D*, 105, 083526
 Gosenca M., Adamek J., Byrnes C. T., Hotchkiss S., 2017, *Phys. Rev. D*, 96, 123519
 Green A. M., Kavanagh B. J., 2021, *Journal of Physics G Nuclear Physics*, 48, 043001
 Green A. M., Liddle A. R., Malik K. A., Sasaki M., 2004, *Phys. Rev. D*, 70, 041502
 Hu W., Sugiyama N., 1996, *ApJ*, 471, 542
 Inman D., Kohri K., 2022, arXiv e-prints, p. arXiv:2207.14735
 Inomata K., Kawasaki M., Mukaida K., Yanagida T. T., 2018, *Phys. Rev. D*, 97, 043514
 Kohri K., Nakama T., Suyama T., 2014, *Phys. Rev. D*, 90, 083514
 Kolb E. W., Tkachev I. I., 1994, *Phys. Rev. D*, 50, 769
 Lacey C., Cole S., 1993, *MNRAS*, 262, 627
 Moradinezhad Dizgah A., Franciolini G., Riotto A., 2019, *J. Cosmology Astropart. Phys.*, 2019, 001
 Planck Collaboration et al., 2020, *A&A*, 641, A6
 Raidal M., Spethmann C., Vaskonen V., Veermäe H., 2019, *J. Cosmology Astropart. Phys.*, 2019, 018
 Ricotti M., Gould A., 2009, *ApJ*, 707, 979
 Sasaki M., Suyama T., Tanaka T., Yokoyama S., 2016, *Phys. Rev. Lett.*, 117, 061101
 Sheth R. K., Mo H. J., Tormen G., 2001, *MNRAS*, 323, 1
 Silk J., 2018, *Phys. Rev. Lett.*, 121, 231105
 Volonteri M., Habouzit M., Colpi M., 2021, *Nature Reviews Physics*, 3, 732

APPENDIX A: DENSITY OF COLLAPSED REGIONS

Equation (2) describes the density evolution of an isolated ellipsoidal top-hat overdensity both before and after collapse in the absence of gravitational forces. We illustrate this evolution in Fig. A1. For each of the three principal axes, the density increases until the axis collapses, after which it decreases again as particles drift back apart. In particular, the ellipsoid's density remains subdominant compared to the cosmic mean density (which includes radiation), so the no-gravity approximation remains valid. This picture suggests that most regions that collapse during the radiation epoch never form virialized structures. Berezhinsky et al. (2013) used a more mathematically precise argument to arrive at the same conclusion.

However, in a realistic scenario, each ellipsoid is embedded in a larger but less overdense ellipsoid. After the collapse of each axis,

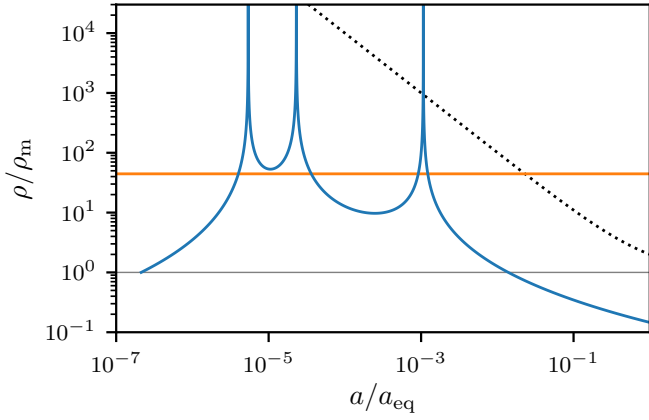


Figure A1. Density evolution for an isolated homogeneous ellipsoid with ellipticity $e = 0.15$ during the radiation epoch. The ellipsoid’s density ρ (blue) significantly exceeds the background matter density ρ_m (thin horizontal line) but does not approach the total density (dotted diagonal line), so it does not become gravitationally bound. Instead, after the collapse of each axis (spikes in the density), the ellipsoid’s material drifts onward, bringing the density back down. In a more realistic picture, however, collapse of successively larger ellipsoids maintains a high density $\sim e^{-2}\rho_m$ (thick orange line) inside the collapsed region, leading to local matter domination, and hence halo formation, around $a \sim 0.02a_{eq}$.

additional material in these larger ellipsoids begins to enter the first ellipsoid, raising its density. In particular, suppose successive ellipsoids i have initial volumes proportional to r_i^3 , so that the fraction of extra mass contributed by the i th ellipsoid beyond that already in the $(i-1)$ th is $(r_i^3 - r_{i-1}^3)/r_{i-1}^3$. Then one way to estimate the density of the collapsed region is to approximate that

$$\frac{\rho}{\rho_m} = \frac{1}{3} \sum_i \frac{\theta(\lambda_1 \delta_i - 1) + \theta(\lambda_2 \delta_i - 1) + \theta(\lambda_3 \delta_i - 1)}{|1 - \lambda_1 \delta_i| |1 - \lambda_2 \delta_i| |1 - \lambda_3 \delta_i|} \frac{r_i^3 - r_{i-1}^3}{r_{i-1}^3}, \quad (\text{A1})$$

where δ_i is the i th ellipsoid’s enclosed linear density contrast and θ is the Heaviside step function. That is, we take each ellipsoid to contribute its density scaled by the fractional mass that it contributes to the system. The latter is just one third per collapsed axis of the total extra mass, $(r_i^3 - r_{i-1}^3)/r_{i-1}^3$, a choice that is easy to justify if we imagine that the ellipsoids are instead initially cubical shells. Note that for simplicity, we also assume that all of the ellipsoids have the same axis ratios.

The linear density contrast δ is related to the primordial curvature fluctuation ζ by Eq. (1). In particular, we can write

$$\delta_i = I_1 \zeta(r_i) \log(I_2 a/a_{H,i}), \quad (\text{A2})$$

where the horizon scaling during radiation domination implies that $a_{H,i} = a_{H,0} r_i / r_0$. As an approximation, let us also write

$$\zeta(r) = \zeta_0 (r/r_0)^{-n} \quad (\text{A3})$$

for some ζ_0 and $n > 0$. We expect that $n \simeq -d \log \Xi_\zeta / d \log r$, where Ξ_ζ is the volume-averaged correlation function

$$\Xi_\zeta(r) = \frac{3}{r^3} \int_0^r r'^2 dr' \xi_\zeta(r') = \int_0^\infty \frac{dk}{k} \mathcal{P}_\zeta(k) W(kr), \quad (\text{A4})$$

where $\xi_\zeta(r)$ is the correlation function of ζ , \mathcal{P}_ζ is the dimensionless power spectrum of ζ , and $W(x) = (3/x^3)(\sin x - x \cos x)$ is the top-hat window function.

We can now take the continuum limit of Eq. (A1) to obtain an

integral,

$$\frac{\rho}{\rho_m} = \int \frac{dr}{r} \frac{\theta(\lambda_1 \delta - 1) + \theta(\lambda_2 \delta - 1) + \theta(\lambda_3 \delta - 1)}{(|1 - \lambda_1 \delta| + \epsilon)(|1 - \lambda_2 \delta| + \epsilon)(|1 - \lambda_3 \delta| + \epsilon)}, \quad (\text{A5})$$

where we add a small parameter $\epsilon > 0$ to ensure convergence. Equations (A2) and (A3) imply

$$\frac{d \log \delta}{d \log r} = -n - \log \left(I_2 \frac{a}{a_{H,0}} \frac{r_0}{r} \right)^{-1} \simeq -n, \quad (\text{A6})$$

where the last approximation is valid in the late-time limit, long after the relevant modes have entered the horizon. In this limit,

$$\frac{\rho}{\rho_m} \simeq \frac{1}{n} \int_0^\infty \frac{d\delta}{\delta} \frac{\theta(\lambda_1 \delta - 1) + \theta(\lambda_2 \delta - 1) + \theta(\lambda_3 \delta - 1)}{(|1 - \lambda_1 \delta| + \epsilon)(|1 - \lambda_2 \delta| + \epsilon)(|1 - \lambda_3 \delta| + \epsilon)}. \quad (\text{A7})$$

Recall that we define $\lambda_1 = (1 + 3e + p)/3$, $\lambda_2 = (1 - 2p)/3$, and $\lambda_3 = (1 - 3e + p)/3$, so ρ/ρ_m is a function of the ellipticity e , prolateness p , and n . This integral can be evaluated analytically, but the resulting expression is complicated. Instead, we comment that the outcome depends only weakly on p , which is typically close to zero, and is well approximated by

$$\frac{\rho}{\rho_m} \simeq \frac{\log_{10}(1/\epsilon)}{ne^2}. \quad (\text{A8})$$

Roughly speaking, ϵ sets the minimum comoving separation of opposite ends of a collapsing ellipsoid, in units of their initial separation. Of course there is physically no minimum, but the resulting regularization of the density can be viewed as a consequence of the finite thickness of the initial phase sheet due to dark matter’s thermal motion. If the dark matter is PBHs, it can be regarded instead as a consequence of the nonzero separation between individual particles. Alternatively, it may be viewed as a choice to neglect the formation of structures too far below the scales we are studying. In any event, for plausible choices of ϵ , the prefactor in Eq. (A8) is of order 1. The correlation slope n is also typically of order 1, so $\rho/\rho_m \sim e^{-2}$ up to a factor of a few. We mark this density in Fig. A1. We also remark that if $\mathcal{P}_\zeta(k)$ is only a shallow function of k , then n could be much smaller than 1, greatly boosting ρ/ρ_m .